PAPER

Benefits of tubular morphologies on electron transfer properties in CNT/TiNT nanohybrid photocatalyst for enhanced H$_2$ production

M. Mamatha Kumari,*[ab] A. Priyanka,[a] B. Marenna,[a] Prathap Haridoss,*[b]
D. Praveen Kumar[a] and M. V. Shankar[a]

In order to study the influence of one dimensional tubular structures for effective electron and hole transportation onto the surface of a photocatalyst leading to efficient solar photocatalytic hydrogen production, functionalized carbon nanotube (FCNT)/TiO$_2$ nanotube nanohybrids were prepared. TiO$_2$ nanotubes (TiNTs) were prepared by hydrothermal method. A series of novel functionalized carbon nanotube/TiO$_2$ nanotube nanohybrids (CTT) were prepared for different wt% (1–20) of FCNTs by wet impregnation method to extend absorption in the visible region and also to retard the electron–hole pair recombination and thereby to enhance the H$_2$ production capability under solar light irradiation. The functionalized carbon nanotube/TiO$_2$ nanotube nanohybrids (CTT) were characterized with XRD, TEM, DRS-UV-Vis, Raman spectroscopy and XPS for crystal structure, morphology, optical properties and chemical composition. Addition of FCNTs to the TiNTs in CTT nanohybrids extended the absorption to the visible region. Relative electron–hole recombination times were measured with photoluminescence spectra. The highest H$_2$ generation of 29 904 µmol g^{-1} was observed after 4 h under optimal conditions due to better separation of electron–hole pairs and electron conducting properties.

Introduction

Since the discovery of carbon nanotubes by Ijima,[1a] they have been of great interest to researchers for their 1D tubular structure, good conductivity, high surface area and unique optical properties[1b,c]. Due to these interesting properties, they have been used as co-catalyst and also as sensitizer in photocatalytic applications such as photodegradation of organic dyes, removing pollutants from air and water, and hydrogen generation from water splitting *etc.*[2] Photocatalysts that generate hydrogen through water splitting by utilizing solar energy, contribute to environmentally friendly programs due to their properties such as zero emissions. Among the photocatalysts, TiO$_2$ is a promising candidate because of its relatively low cost, non-toxicity, stability and suitable band edge positions for redox reactions.

Among several nanocrystalline structures of TiO$_2$ photocatalysts, TiO$_2$ nanotubes (TiNT) have more optimal properties for photocatalytic H$_2$ production due to their one dimensional nanostructure. Previous studies have shown that combination of TiNT with other nanomaterials have increased photocatalytic activity.[3]

Several studies[4] have been carried out to utilize CNTs in improving the photocatalytic H$_2$ production efficiency of TiO$_2$ nanoparticles in view of their unique optical and electron transport properties. Silva *et al.*[5a] studied the photocatalytic H$_2$ production of MWCNT/TiO$_2$ photocatalyst from aqueous methanol and saccharide solutions. Recently Tarigh *et al.*[5b] reported a simple, effective and recoverable photocatalyst MWCNT/TiO$_2$ for enhanced photocatalytic activity. There is still a significant potential for improvement in the photocatalytic activity of all the above photocatalysts by reducing the electron–hole recombination through one dimensional nanostructure.[7] This motivated us to study effect of one dimensional nanostructure of both CNTs and TiNTs on the photocatalytic H$_2$ production under solar irradiation.

Also, less attention has been paid to synthesis of CNT/TiNT nanohybrid and its photocatalytic activity. Doong *et al.*[6] studied degradation efficiency of CNT/TiNT composite and found that it is a promising nano-adsorbent for coupled removal of organic as well as heavy metal ions in solution. However, to the best of our knowledge research work on CNT/TiNT (TiO$_2$ nanotubes) nanohybrid for hydrogen generation under natural solar light by water splitting, is scarce.

In the present work we study the preparation method for CNT/TiNT nanohybrid and its hydrogen generation efficiency under natural solar light irradiation by water splitting.

[a]Nanocatalysis and Solar Fuels Research Laboratory, Department of Materials Science & Nanotechnology, Yogi Vemana University, Kadapa-516 003, Andhra Pradesh, India. E-mail: mamatha@yogivemanauniversity.ac.in; Tel: +91-8886577869

[b]Department of Metallurgical and Materials Engineering, Indian Institute of Technology Madras, Chennai 600 036, Tamil Nadu, India. E-mail: prathap@iitm.ac.in; Tel: +91-9444468235

Experimental methods

Materials

All the chemicals used for the present work are of analytical grade and the details of the chemicals and catalysts used are given below. Commercial titanium dioxide TiO_2 P-25 catalyst (anatase 80%, rutile 20%, surface area = 50 m^2 g^{-1} and particle size 27 nm) was received from Degussa Corporation, Germany. Commercial TiO_2 (particle size $\approx$ 150 nm, surface area = 5.1 m^2 g^{-1}, LAB) used for nanotube synthesis was purchased from Merck, India. Sodium hydroxide pellets (99%), hydrochloric acid (35%), HNO$_3$ (33%), H$_2$SO$_4$ (38%) and glycerol (98%) were received from Merck, India. De-ionized water (100%, battery grade) used for synthesis, impregnation process and photo-catalytic experiments was procured from LIMRA, Kadapa, India.

Synthesis of FCNTs

Carbon nanotubes were synthesized by arc discharge method in open air.[4e] Functionalization of CNTs has been described in detail in an earlier report.[4e] Briefly functionalization of CNTs was carried out to remove amorphous carbon, metal catalyst and also to introduce acid functional groups to the carbon nanostructures, by ultrasonicating them in 3 : 1 volume ratio mixture of H$_2$SO$_4$/HNO$_3$ at 40 °C for 2 h, followed by washing with plenty of water till reaches pH $\approx$ 7 and drying at 80 °C overnight.

Synthesis of TiNTs

TiO_2 nanotubes (TiNTs) were prepared by alkaline hydro-thermal method.[4f] Briefly, the synthesis process involves dispersion of 2.5 g of TiO_2 (Merck) in 10 M NaOH solution and cooking in 250 mL Teflon lined stainless steel autoclave at 100–130 °C for 20–24 h. The white slurry obtained was then washed with distilled water, later by dilute HCl, finally washed with ethanol and dried at 80 °C. Dried powder was subjected to calcination at 350 °C for 3 h to get TiNT.

Synthesis of FCNTs/TiNTs nanohybrid

TiO_2 nanotubes/FCNT nanohybrid photocatalysts were prepared through wet impregnation method. Functionalized CNTs (FCNTs) and hydrothermally synthesized TiNTs were taken as starting materials. In a typical impregnation procedure, required amount (1–20 wt%) of FCNTs (Table 1) was dispersed in ethanol aqueous solution in beaker-1,

Table 1 Photocatalysts used

Photocatalyst	Nomenclature
Functionalized carbon nanotubes	FCNT
TiO_2 nanotube	TiNT
1 wt% FCNT loaded TiNT	CTT-1
2 wt% FCNT loaded TiNT	CTT-2
10 wt% FCNT loaded TiNT	CTT-10
20 wt% FCNT loaded TiNT	CTT-20

ultrasonicated and magnetically stirred for 1 h. Simultaneously, in beaker-2, TiNT was dispersed in ethanolic aqueous solution. Then contents in beaker-1 was transferred into beaker-2 and resulting mixture was ultrasonicated for 1 h. The TiNT/FCNT mixture containing ethanolic aqueous solvent, was subjected to heating and magnetic stirring till the solution is completely evaporated. Nanohybrid mixture was kept for drying in oven at 80 °C overnight and calcination in tubular furnace in air at 450 °C for 2 h, with a heating rate of 5 °C min^{-1}.

Characterization

Transmission Electron Microscopy (TEM) images were recorded on a PHILIPS instrument (120 kV). The powder catalyst samples for TEM observations were directly deposited onto carbon coated Cu-grids. The XRD patterns were recorded on Siemens D-5000 X-ray diffractometer (2θ = 20–90°). Thermo gravimetric analysis (TGA) was performed on a universal instrument using TGA Q 500 analyzer with a heating rate of 10 °C min^{-1} under nitrogen flow. Diffuse Reflectance UV-Visible spectra were recorded on a GBC UV-Visible Cintra 10e spectrometer, in the wavelength range 200–500 nm. X-ray photoelectron spectra (XPS) were recorded on a KRATOS AXIC 165 equipped with Mg K$_\alpha$ radiation. Confocal Raman spectra of all the samples were recorded using Raman spectrometer (RENISHAW) operating with an excitation wavelength of 532 nm and a power 1 mW. Photoluminescence (PL) spectra were recorded using Spectro-fluorometer, (FLUORA MAX 4P) excitation wavelength at 320 nm.

Photocatalytic H$_2$ production activity

Photocatalytic hydrogen evolution reactions were carried out in a 150 mL quartz reactor sealed using an air-tight rubber septum to keep the experimental set up leak-proof and enable gas sampling. Typically, 5 mg of catalyst was suspended in 50 mL of a 5 vol% glycerol aqueous solution. Prior to solar experiments, the catalyst suspension was stirred in dark for 30 min followed by degassing and purging with nitrogen (high pure) gas to eliminate oxygen from the reaction system. Catalytic activities were performed under continuous magnetic stirring and solar light was used to excite the photocatalyst for red-ox reaction on the catalyst surface. The amount of H$_2$ and O$_2$ produced was measured by offline gas chromatography. Control experiments were carried out under similar experimental conditions in the absence of photocatalyst or sun light, neither H$_2$ nor O$_2$ gas was detected.

Results and discussion

X-ray diffraction

Fig. 1 presents the XRD patterns of TiNT, CTT-1, CTT-2, CTT-10, CTT-20 and FCNT photocatalysts. FCNT showed a broad peak located between 20° and 30° which is assigned to the (002) plane of the carbon structure. The diffraction peaks of TiO_2 were identified with reference to JCPDS database. The photocatalysts TiNT, CTT-1 and CTT-2 displayed diffraction peaks at 2θ = 25.3°, 37.8°, 48.0°, 53.8°, 54.9° and 62.5° which are the peaks of
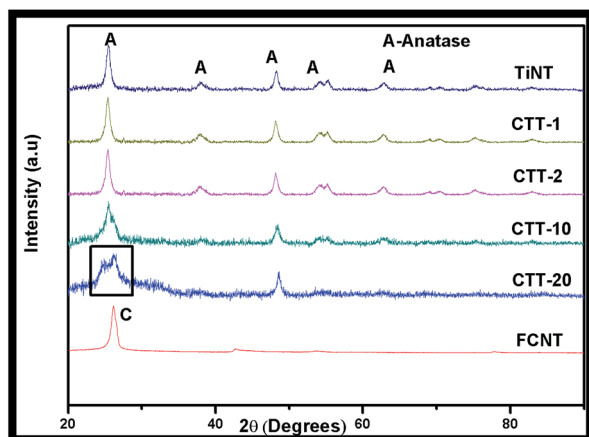
Fig. 1 XRD patterns of TiNT, CTT-1, CTT-2, CTT-10, CTT-20 and FCNTs.

(101), (004), (200), (105), (211) and (204) respectively for anatase phase (JCPDS 21-1272). Also, with increase in FCNT content, a new peak at 26.2° is observed clearly for CTT-20 corresponding to the carbon (100) in FCNT. Carbon (100) peak is not observed in CTT-2 and slightly in CTT-10, due to the presence of lower amount of FCNT. Kim et al.,[8a] studied TiO_2 nanoparticle loaded on graphene/carbon nanocomposites photocatalysts and XRD pattern displayed characteristic peaks of anatase-rutile phases in addition to carbon nanostructures. We have also observed characteristic XRD peaks of both TiO_2 anatase-rutile and carbon in FCNTs/TiO_2 nanoparticles nanohybrid material.[4e] The results reveal that addition of FCNTs to TiO_2 nanotubes suppressed both grain growth and phase transformation. This is mainly attributed to fine dispersion of TiO_2 nanotubes on FCNTs surface.

TEM

TEM image Fig. 2 shows the as-prepared CTT-2 nanohybrid. Fig. 2(a) shows that bundles of TiO_2 nanotubes of lengths 100–

500 nm are dispersed on the FCNTs whose diameters are in the range of 30–50 nm. As both FCNTs and TiNTs are tubular structure, in order distinguish one from the other, rectangle marked region is magnified as shown in Fig. 2(b). Further, HRTEM image Fig. 2(c) showing the lattice spacing of TiNT is subjected to profile of live FFT image Fig. 2(d) to measure the observed interplanar spacing. Measured lattice spacing from live FFT is 0.352 nm which is approximate to that of (101) anatase TiO_2. This is further confirmed by the SAED pattern shown in the inset of Fig. 2(c).

UV-Visible DRS

Optical properties of the prepared nanohybrids CTT-1, 2,10, 20 & TiNT were studied by analyzing UV-Visible Diffuse Reflectance spectrum (Fig. 3(a)). It is seen that CTT-1, 2,10 & 20 showed enhanced absorption towards visible region than TiNT. Approximate absorption edges of CTT-1, 2,10 & 20 are in the order 395, 424, 413 and 449 nm while that of TiNT is 389 nm. A clear red shift of the absorption lengths can be attributed to presence of FCNTs in the nanohybrid. It is observed that CTT-2 showed higher absorption and absorption edge than CTT-10 and CTT-20. This increased absorption in visible region could also be due to $\pi \rightarrow \pi^*$ of CNT and $n \rightarrow \pi^*$ between n-orbit of oxygen species of TiNT.[8b-d]

Kubelka–Munk plot (Fig. 3(b)) shows that the band gap values of CTT nanohybrids are reduced to 2.98 eV from a value
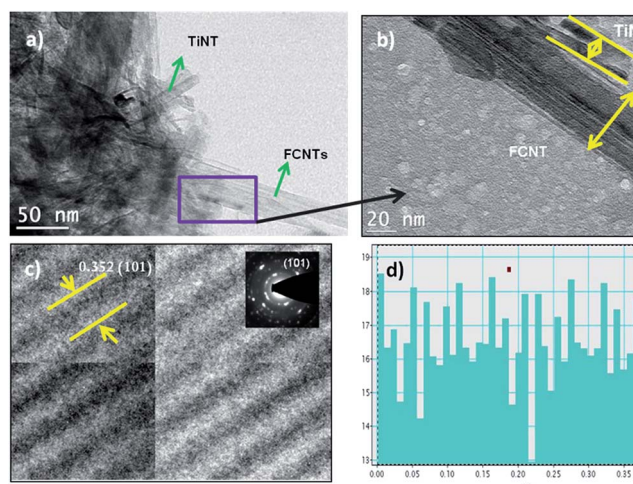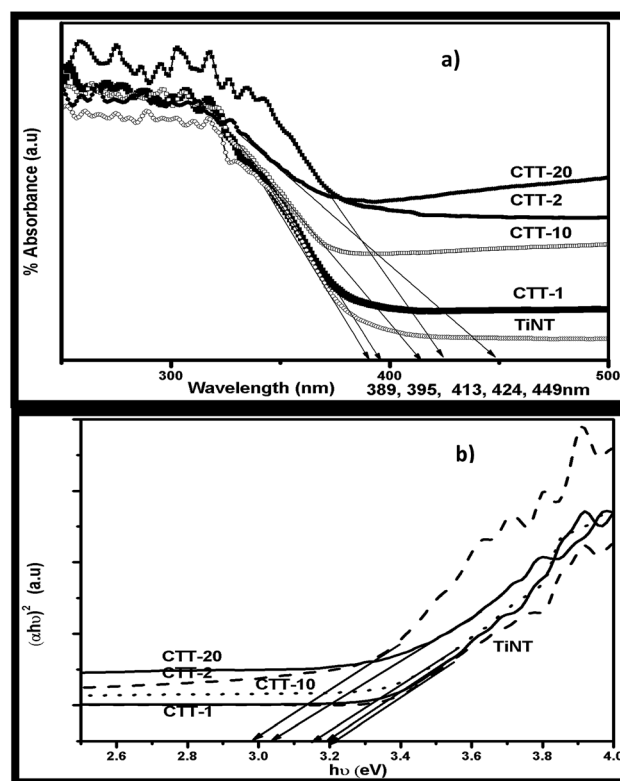

Fig. 2 TEM and HRTEM images of TiO_2 nanotube/FCNT nanohybrid (a), (b) showing the morphological structure (c), (d) showing the interplanar spacing and live FFT image respectively.

Fig. 3 (a) UV-Vis DRS and (b) transformed Kubelka−Munk functions $(\alpha h\nu)^2$ vs. photon energy ($h\nu$, eV) of CTT-1, 2, 10, 20 & TiNT photocatalysts.

3.2 eV of TiNT. This decrease in band gap energies is due to synergetic effect of presence of FCNTs attached to the surface of TiNT rather than occupying lattice sites in the nanohybrid.[8e]

XPS analysis

XPS analysis was performed on prepared CTT-2 and the wide scan spectrum (Fig. 4(a)) contains Ti 2p, O 1s and C 1s of TiO_2. High resolution XPS of Ti 2p shows (Fig. 4(b)) intense peaks at 459.70 eV and 460.2 eV corresponding to $2p_{3/2}$ and second highest peak at 465.9 eV corresponding to $2p_{1/2}$, indicating the presence of Ti^{4+} in the nanohybrid. Also, these binding energies are slightly shifted from the corresponding original binding energies at 458.7 eV and 464.5 eV in TiO_2. Such results were reported earlier indicating the strong interaction between TiO_2 nanoparticles and CNTs.[9a,b] O 1s region is composed of two peaks (Fig. 4(c)). Peaks at BE 530.5 eV and 532.7 eV correspond to bulk oxygen in Ti–O–Ti and surface oxygen from the hydroxyl group Ti–OH.

XPS of CTT-2 curve has peaks at 285.4 eV, 286.2 eV and 288.5 eV corresponding to the C–O, C=O and –COO (Fig. 4(d)). Binding energy peaks around 286 eV and 288 eV were attributed to C–O and C=O bonds. This indicates the formation of carbonated structures and probable Ti–O–C bonding.[9c] The interaction of TiNT with FCNTs was further studied using Raman analysis.

Raman analysis

Raman spectrum of CTT-2 is shown in the Fig. 5(a). Characteristic bands at 1326 cm^{-1} and 1579 cm^{-1} in CTT-2 corresponds to D and G bands of CNTs respectively. The relative intensity ratio of D band to G band (I_D/I_G), known as index of graphitization, is found to be 1.1 for CTT-2 nanohybrid while that of CNTs is 0.7.

This indicates that functionalization in acid mixture and calcination temperature during nanohybrid formation did not significantly alter the CNT structure in the nanohybrid. Dai *et al.* also reported an I_D/I_G ratio of 0.78 for MWNT–TiO_2, comparable to that of the pure MWNTs (0.70), indicating that the graphitic structure of MWNTs in the nanocomposites did not change much after functionalization in nitric acid or during the hydrothermal treatment.[9d] The new peak observed at 1616 cm^{-1} (Fig. 5(b)) is due to the interaction between FCNTs and TiNTs. This is in agreement with reported results.[9e]

BET surface area

The surface area of the TP, TiNT and CTT nanohybrid photocatalysts are as shown in the Table 2. An increase in the surface area of the catalyst with increase in ratio of FCNTs to TiNT, is observed. Generally addition of FCNTs reduces the agglomeration of TiO_2.[10a] This property of FCNTs ensures the higher surface area of the nanohybrid with increase in FCNTs addition. The decrease in photocatalytic activity of the CTT-10, CTT-20 is due to high surface area where CNTs become recombination centers for the generated electron–hole pairs and is confirmed by the PL spectra.
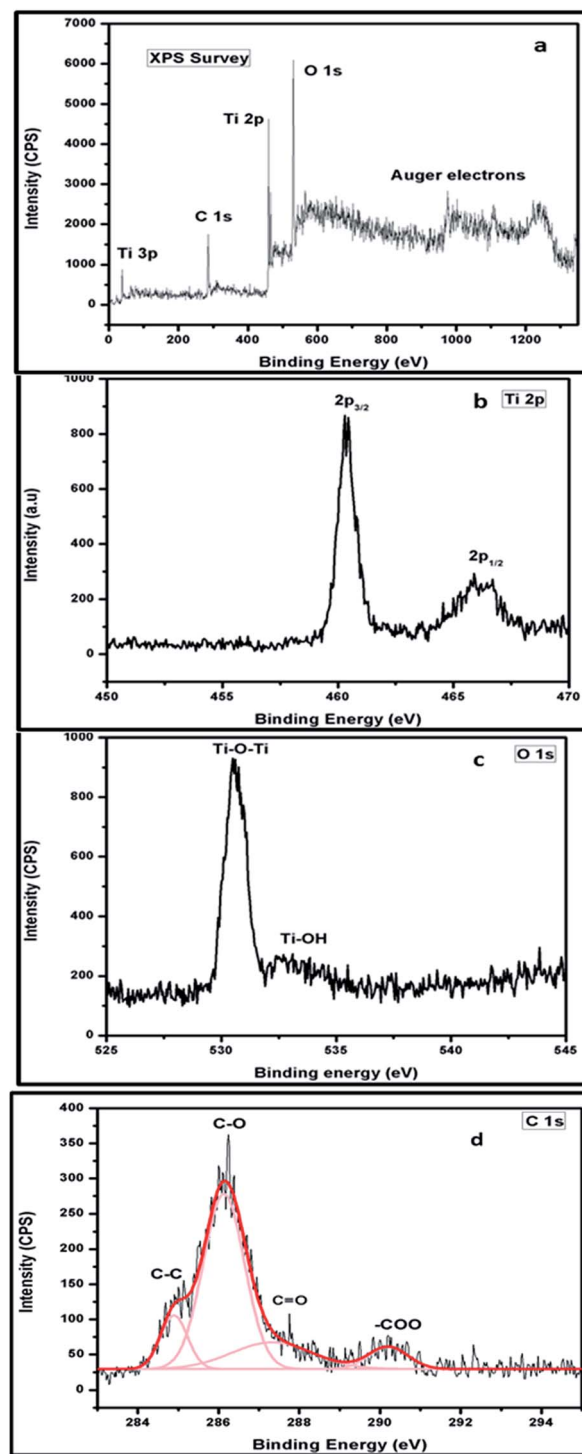

Fig. 4 (a) XPS wide CPS scan (b) Ti 2p (c) O 1s (d) C 1s of CTT-2.

Photoluminescence spectra

Fig. 6 displays the PL spectra of TiNT, CTT-1, -2, -10 & 20 in the wavelength range of 350–550 nm. TiNT showed broad spectrum centred around 375 nm, whereas the nanohybrid catalysts showed decrease in peak intensity in the following order CTT-1 < CTT-2 < CTT-10 < CTT-20. The CTT-20 catalyst displayed blue shift in PL intensity which is attributed to the decrease in TiO_2
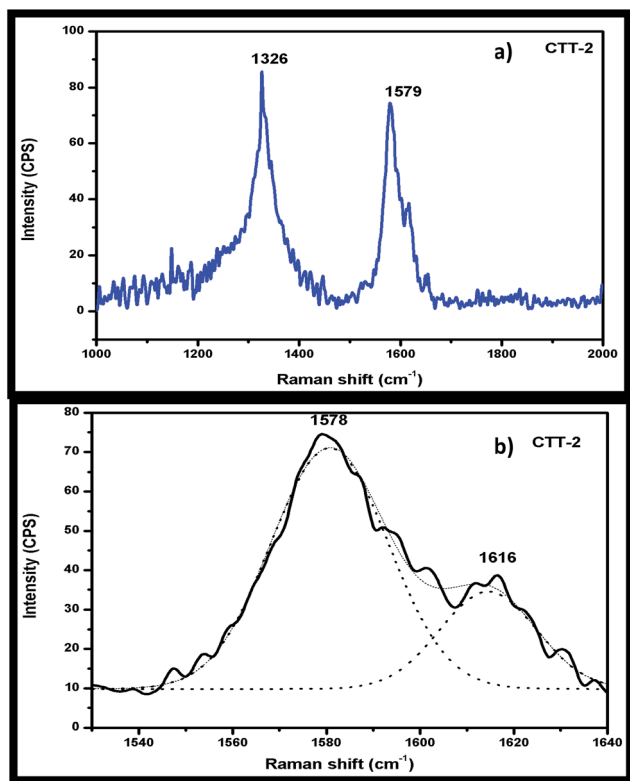
Fig. 5 (a) Raman spectra of CTT-2 catalyst and (b) its expanded view from 1500 to 1640 cm^{-1}.

Table 2 BET surface area of TiNT and CTT photocatalysts

S. No.	Nanohybrid	S_{BET} (m^2 g^{-1})
1	CTT-1	121.8
2	CTT-2	120.5
3	CTT-10	169.5
4	CTT-20	193.6
5	TiNT	70.2
6	TP	50

showed enhanced and almost similar activity. This enhancement may be attributed to higher surface area of FCNT and better bonding of FCNT and TiNT. H_2 production activity of CTT-10 showed lower solar photocatalytic H_2 production than unmodified TiNT due to losses in light absorption and electron–hole recombination. Among CTT nanohybrids CTT-2 showed highest H_2 production of 7476 μmol h^{-1} g^{-1}.

CTT nanohybrid also shows increase in H_2 production activity due to FCNT acting as both co-catalyst and sensitizer. However (TiO_2 nanotubes/FCNTs) CTT samples showed higher activity compared to other TiO_2/MWCNTs photocatalyst[4a,b,e] reported in literature mainly due to the following reasons. Formation of Ti–O–C at the interface of TiO_2 and FCNTs favours the effective charge transfer between them. Also, the 1D tubular structures of TiO_2 nanotubes, in addition to the FCNTs, which allowed uni-directional flow of electrons, hence reducing electron–hole recombination.

Photocatalytic stability

Fig. 8 depicts amount of the H_2 production tested for 4 h in 4 cycles of study. These results reveal that almost identical amount of the H_2 generation was recorded in the all the four experiments. The minor decrease in the total H_2 generation was observed in 3rd and 4th cycles which can be attributed to the poor surface interaction of reaction intermediates formed during oxidation of glycerol in solution. These intermediates could have been adsorbed onto the surface of the photocatalyst which influenced the light penetration to the surface and resulted decrease in the rate of the H_2 production. The stability of TiNTs under recycling conditions was reported elsewhere for
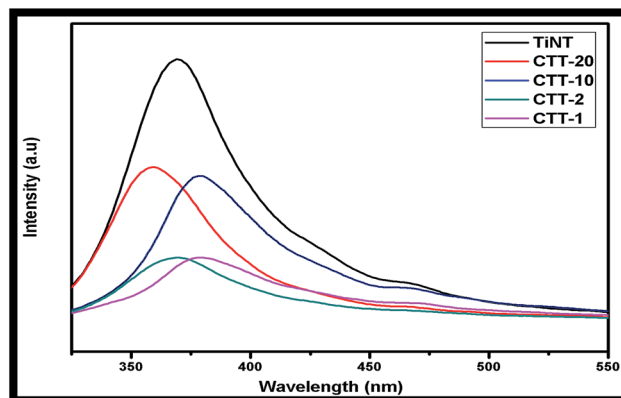
component in nanohybrid catalyst. These results suggest that drastic reduction of charge carrier recombination with associated reduction of PL-intensity. Both CTT-1 and CTT-2 have lower peak intensity and hence showed higher rate of H_2 production (*vide supra*). Kim et al.,[8a] compared the PL intensity of TiO_2/graphene carbon nanocomposites with TiO_2 itself, and they explained that strong interaction between excited electrons on TiO_2 particles and graphene diminished the peak intensity of nanocomposites, this phenomenon was attributed to decrease in charge carrier recombination.

Praveen Kumar et al., observed decrease in PL peak intensity with Cu_2O sensitized TiO_2 nanorods with nanocavities. They concluded that decrease in peak intensity is due to lower recombination rate of charge carriers localized in nanocavities of TiO_2 nanorods.[4f] These results are in agreement with earlier reports.[10a,b]

Photocatalytic H_2 production activity

The photocatalytic performance of the FCNT/TiO_2 nanotube was evaluated by H_2 evolution in the presence of 5 vol% glycerol aqueous solution, which is the sacrificial reagent, under natural solar irradiation. Fig. 7 shows the H_2 production activity of TiNT, CTT-1, 2, 10 & 20 photocatalysts with increase in solar irradiation time. Linear increase in the H_2 production activity of all the photocatalysts is observed with increase in time.

H_2 production activity is enhanced with the addition of FCNT to TiNT. Also, H_2 production activity of CTT-1 and CTT-2

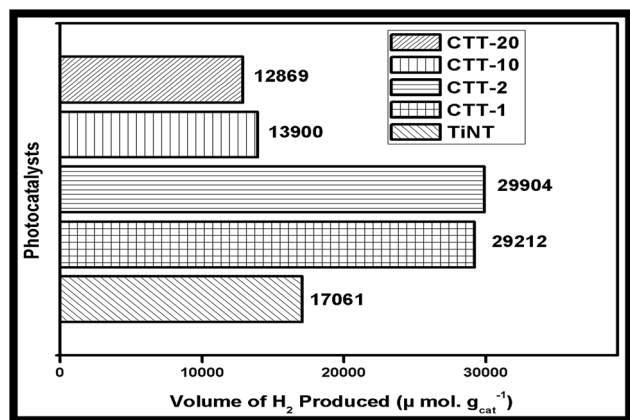**Fig. 6** PL spectra of TiNT, CTT-1, CTT-2, CTT-10 & 20.

Fig. 7 Comparison of H_2 production activity of TiNT, CTT-1, 2 & 10 photocatalysts under solar irradiation for 4 h.

the enhanced rate of H_2 production under solar and visible light irradiation.[10c,d]

Structure activity correlation

Based on the characterization results of the data it is evident that impregnation of FCNTs with TiNT's resulted in well dispersed catalysts and indicates strong interaction of FCNTs with TiNT. Electrons and holes get generated as the nanohybrid is exposed to sunlight in the conduction and valence bands respectively. Improvement in the visible light absorption and decreased band gap energy values of the nanohybrid could be due to the creation of intermediate energy levels of doped FCNTs. The possible photoexcitation and charge transfer processes are as shown in the Fig. 9. Lu *et al.*, deduced that band gap is probably reduced as a result of doping state creation near to the E_F.[10e] The electrons accumulated on the conduction band of TiNT could be transferred to H^+ to produce H_2 while holes in the valence band of TiNT are consumed by the sacrificial agent glycerol which subsequently gets mineralized leading to suppression of recombination of photogenerated charge carriers and enhancement of H_2 production.
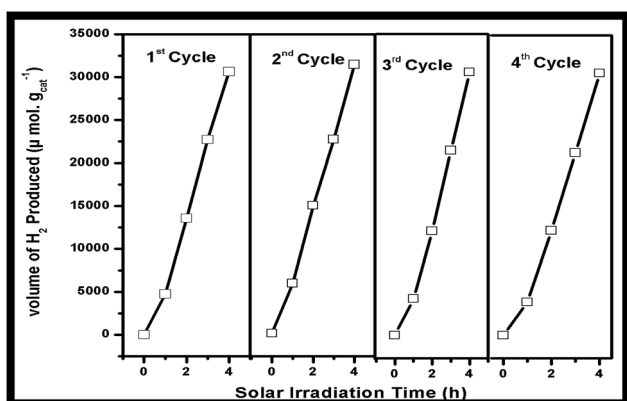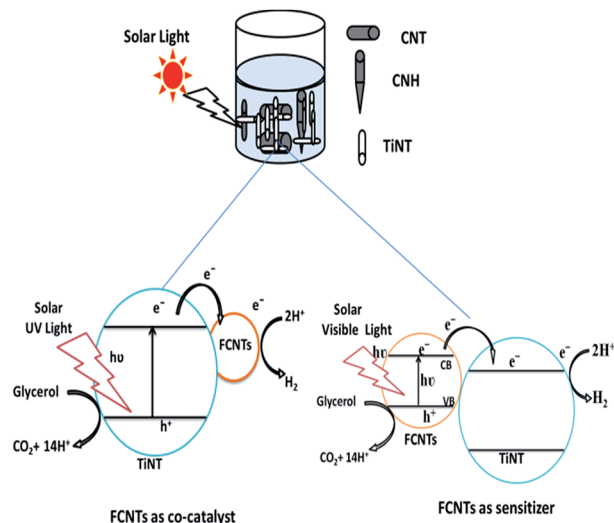

Fig. 9 Schematic illustration of mechanism of FCNTs under solar irradiation.

Conclusions

In conclusion this work resulted in synthesis of a series of novel functionalized carbon nanotube/TiO_2 nanotube nanohybrid materials by wet impregnation method to extend absorption to the visible region and also to retard the electron–hole pair recombination and thereby to enhance the H_2 production capability under solar light irradiation. The percentage addition of FCNTs to TiNTs influences the photocatalytic activity of CTT composite. Highest photocatalytic H_2 production was observed for CTT-2 photocatalysts mainly due to extension of absorption edge to the visible region and also by retardation of electron–hole recombination as compared to other photocatalysts.

Acknowledgements

Fig. 8 H_2 production activity in 4 cycles using 5 mg CTT-2 catalysts under solar irradiation.

References

1 (*a*) S. Ijima, *Nature*, 1991, **354**, 56–58; (*b*) P. Rima, Z. Kumbhakara and A. K. Mitra, *J. Mater. Sci. Eng. B*, 2010, **167**, 97–101; (*c*) A. Profumo, M. Fagnoni and D. Merli, *J. Anal. Chem.*, 2006, **78**, 4194–4199.

2 (*a*) K. Woan, G. Pyrgiotakis and W. Sigmund, *Adv. Mater.*, 2009, **21**, 2233–2239; (*b*) P. Serp and J. L. Figueiredo, *Carbon Materials for Catalysis*, Wiley, 2009, pp. 481–506; (*c*) Y. K. Kim and H. Park, *Energy Environ. Sci.*, 2011, **4**, 685–694.

3 (*a*) T. S. Natarajan, K. Natarajan, H. C. Bajaj and J. T. Rajesh, *J. Nanopart. Res.*, 2013, **15**(1669), 1–18; (*b*) G. Zhang, H. Huang, W. Li, F. Yu, H. Wu and L. Zhou, *Electrochim. Acta*, 2012, **81**, 117–122; (*c*) Y. Qin, G. Wang and Y. Wang, *Catal. Commun.*, 2007, **8**, 926–930.

4 (*a*) W. Wang, P. Serp, P. Kalck and J. L. Faria, *Appl. Catal., B*, 2005, **56**, 305–312; (*b*) G. An, W. Ma, Z. Sun, Z. Liu, B. Han, Z. Miao and K. Ding, *Carbon*, 2007, **45**, 1795–1801; (*c*) C. Song, P. Chen, C. Wang and L. Zhu, *Chemosphere*, 2012, **86**, 853–859; (*d*) Y. Ou, J. Lin, S. Fang and D. Liao, *Chem. Phys. Lett.*, 2006, **429**, 199–203; (*e*) M. Mamatha Kumari, D. Praveen Kumar, P. Haridoss, V. Durga Kumari and M. V. Shankar, *Int. J. Hydrogen Energy*, 2014, **40**, 1665–1674; (*f*) D. Praveen Kumar, N. Lakshmana Reddy, M. Mamatha Kumari, B. Srinivas, V. Durga Kumari, B. Sreedhar, V. Roddatis, O. Bondarchuk, M. Karthick, B. Nepolian and M. V. Shankar, *Sol. Energy Mater. Sol. Cells*, 2015, **136**, 157–166.

5 (*a*) C. G. Silva, M. J. Sampaio, R. R. Marques, L. A. Ferreira, P. B. Tavares, A. M. Silva and J. L. Faria, *Appl. Catal., B*, 2015, **178**, 82–90; (*b*) G. D. Tarigh, F. Shemirani and N. S. Maz'hari, *RSC Adv.*, 2015, **5**, 35070–35079.

6 (*a*) S. Dong, H. Wang and Z. Wu, *J. Phys. Chem. C*, 2009, **113**, 16717–16723; (*b*) R. A. Doong and L. F. Chiang, *Water Sci. Technol.*, 2008, **58**, 1985–1992.

7 (*a*) A. Miribangul, X. Ma, C. Zeng, H. Zou, Y. Wu, T. Fan and Z. Su, *Photochem. Photobiol.*, 2016, **92**, 523–527; (*b*) S. Xiao, W. Zhu, P. Liu, F. Liu, W. Dai, D. Zhang, W. Chen and H. Li, *Nanoscale*, 2016, **8**, 2899–2907.

8 (*a*) K. M. Kim, H. O. Pae, M. Zheng, R. Park, Y. M. Kim and H. T. Chung, *Circ. Res.*, 2007, **101**, 919–927; (*b*) C. Lettmann, K. Hildenbrand, H. Kisch, W. Macyk and W. F. Maier, *Appl. Catal., B*, 2001, **32**, 215–227; (*c*) Y. Aoki, K. Urita, D. Noguchi, T. Itoh, H. Kanoh and T. Ohba, *Chem. Phys. Lett.*, 2009, **482**, 269–273; (*d*) M. Inagaki, M. Nonaka, F. Kojin, T. Tsumura and M. Toyoda, *Environ. Sci. Technol.*, 2006, **27**, 251–258; (*e*) Y. Xie, S. H. Heo, S. H. Yoo, G. Ali and S. O. Cho, *Nanoscale Res. Lett.*, 2010, **5**, 603–607.

9 (*a*) G. An, W. Ma, Z. Sun, Z. Liu, B. Han and S. Miao, *Carbon*, 2009, **47**, 1795–1801; (*b*) C. Song, P. Chen, C. Wang and L. Zhu, *Chemosphere*, 2012, **86**, 853–859; (*c*) S. K. Parayil, H. S. Kibombo, C. M. Wu, R. Peng, T. Kindle and J. Baltrusaitis, *J. Phys. Chem. C*, 2010, **117**, 16850–16862; (*d*) K. Dai, T. Peng, D. Ke and B. Wei, *Nanotechnology*, 2009, **20**, 125603–125609; (*e*) Y. Yu, J. C. Yu, J. Yu, Y. Kwok, Y. Che and J. Zhao, *Appl. Catal., A*, 2005, **289**, 186–196.

10 (*a*) C. Hyo and B. Kim, *Carbon*, 2012, **50**, 2472–2481; (*b*) X. J. Lv, S. X. Zhou, C. Zhang, H. X. Chang, Y. Chena and W. Fu, *J. Mater. Chem.*, 2012, **22**, 18542–18549; (*c*) D. Praveen Kumar, M. V. Shankar, M. Mamatha Kumari, G. Sadanandam, B. Srinivas and V. Durga Kumari, *Chem. Commun.*, 2013, **49**, 9443–9445; (*d*) K. Lalitha, G. Sadanandam, V. Durga Kumari, M. Subrahmanyam, B. Sreedhar and Y. Hebalkar Neha, *J. Phys. Chem. C*, 2010, **114**, 22181–22189; (*e*) S. Y. Lu, C. W. Tang, Y. H. Lin, H. F. Kuo, Y. C. Lai, M. y. Tsai, H. Ouyang and K. Hsuw, *Appl. Phys. Lett.*, 2010, **96**, 231915–231923.